

Three dimensional meshless point generation technique for complex geometry

*Jae-Sang Rhee¹⁾, Jinyoung Huh²⁾, Kyu Hong Kim³⁾, Suk Young Jung⁴⁾

^{1),2)} *Department of Mechanical & Aerospace Engineering, Seoul National University*

³⁾ *Department of Mechanical & Aerospace Engineering/Institute of Advanced Aerospace Technology, Seoul National University*

⁴⁾ *Agency for Defense Development*

¹⁾ jsrhee@snu.ac.kr

ABSTRACT

This study aims to develop meshless point generation technique which can be applied to complex geometry. Generally, grid generation for FVM requires a large amount of time and labor. However, the point generation technique developed in this research enables the points to be generated automatically in the regime of interest. Consequently, time required for generation of computational domain can be shortened, as compared to that of FVM. Numerical analysis of three-dimensional inviscid flow around the body of NASA TM X 2059 model was done for the validation of the developed point generation technique. The model was supplemented with four tail fins and Twenty-Degree conical nozzle with four vanes. Least square method was selected for spatial discretization and LU-SGS method was also adopted for time discretization. In addition, Minmod limiter modified for Meshless method was utilized for accurate calculation. The result shows that the point generation technique for Meshless method is available on external flow of complex geometry together with nozzle.

1. INTRODUCTION

A meshless method is a newly suggested computational fluid dynamics (CFD) algorithm in recent years. This method requires only neighboring points of each point without mesh. Therefore it is less restrictive when generating the computational domain around a complicated or moving geometry than the mesh based method. A meshless method was introduced in 1977 at first. Since then, a variety of Meshless algorithms

^{1),2)} Graduate student

³⁾ Professor

⁴⁾ Ph.D.

have been studied by former researchers. Since 2000, meshless algorithms which analyze compressible flow using moving least square method (LSM) have been developed by Katz (2009) respectively and so on. However, previous researchers have focused on two dimensional flow until now. In order to analyze three dimensional complicated flow field, much more intensified effort to generate computational points around a complex geometry is necessary. As a method to this problem, efficient and robust three dimensional meshless point generation algorithm is developed in this study. For a validation, this algorithm was applied to NASA X TM 2059 with a nozzle and vanes that is considered as complex geometry. Then using generated point system, computation of flow fields was conducted by the meshless code for compressible flow developed by Huh (2013). Least square method and AUSMPW+ (Kim 2001) was adopted for the spatial discretization, LU-SGS was adopted for the time integration. Results were shown comparing with ones from unstructured method by FLUENT.

2. POINT GENERATION ALGORITHM

The generation process of the meshless point system consists of two steps. The first step is the near surface point generation and the second step is the background point generation. The generation of the near surface point algorithm is based on the electric potential theory. And the background point is generated from Cartesian grid point

2.1 Near surface points generation

The near surface points are created along the electric field lines which are generated from the points on the surface. Assume that the points on the surface have charge, the electric field generated from a set of point charge on the surface is derived from Coulomb's law. It is shown in Eq. (1)

$$\begin{aligned} E_{x,i} &= \sum_j \frac{k_j}{d^2} (x_{s,j} - x_i) \\ E_{y,i} &= \sum_j \frac{k_j}{d^2} (y_{s,j} - y_i) \\ E_{z,i} &= \sum_j \frac{k_j}{d^2} (z_{s,j} - z_i) \end{aligned} \quad (1)$$

In Eq. (1), $E_{x,i}$, $E_{y,i}$, $E_{z,i}$ are x, y, z component of the electric field at point i which exists outside the surface, $x_{s,j}$, $y_{s,j}$, $z_{s,j}$ are x, y, z-coordinate of surface point charge which has index j , x_i , y_i , z_i are x, y, z-coordinate of the point i , d is the distance between point i and j , and k_j is the constant which is determined by users. The electric field line can be obtained by Eq. (1). The example of near surface point system generated is illustrated in Fig. 1

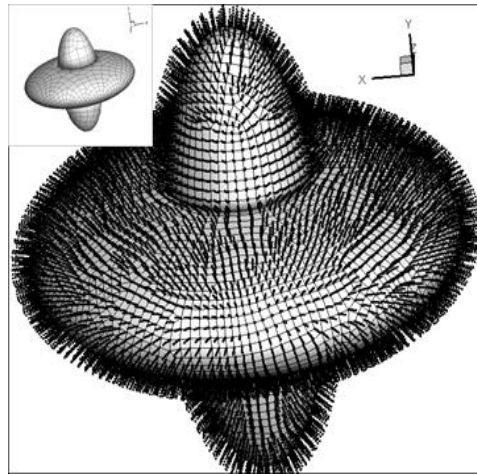


Fig. 1 The near surface points of UFO shaped object

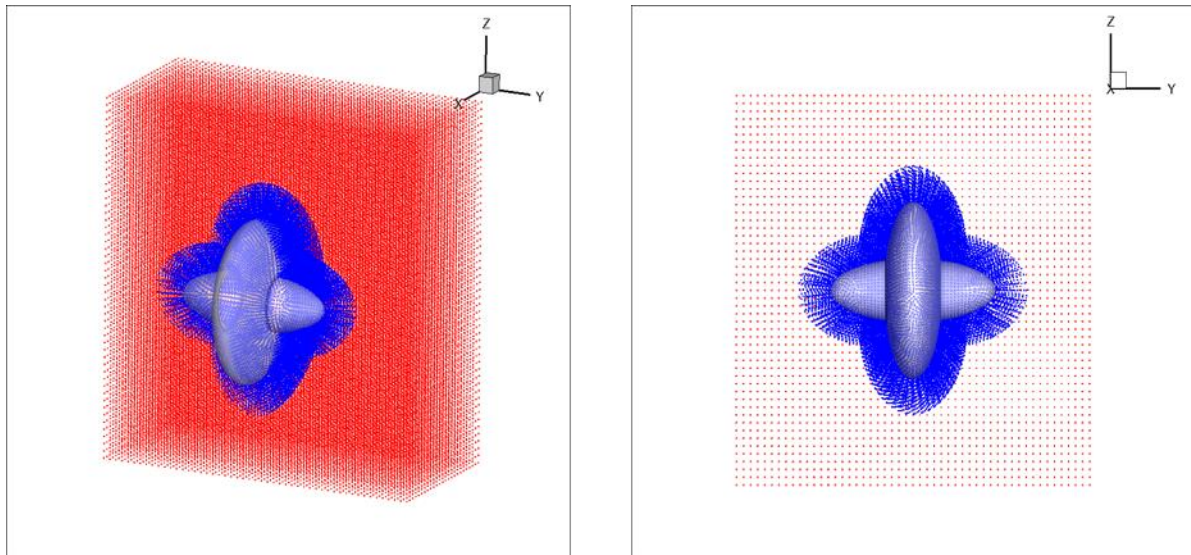


Fig. 2 The total point system of UFO shaped object

2.2 Background points generation

The background points are generated from Cartesian grid point. Consider Cartesian grid, Let the interval of x , y and z direction be $\Delta x, \Delta y, \Delta z$. And let the number of points of x , y and z direction be N_x, N_y, N_z . Then the coordinates of Cartesian grid points are denoted as follow.

$$\begin{aligned}
 x_{i,j,k} &= x_{ini} + (i - 1)\Delta x, & (1 \leq i \leq N_x) \\
 y_{i,j,k} &= y_{ini} + (j - 1)\Delta y, & (1 \leq j \leq N_y) \\
 z_{i,j,k} &= z_{ini} + (k - 1)\Delta z, & (1 \leq k \leq N_z)
 \end{aligned} \tag{2}$$

In Eq. (2), x_{ini} , y_{ini} , and z_{ini} are initial point where i , j , and k are 1. From Cartesian grid points, the background point system are generated. The total point system is accomplished by eliminating the background points inside the near surface points. It is illustrated in Fig 2.

3. LOCAL POINTS CLOUD CONFIGURATION STRATEGY

In order to use the least square method, every computational points must be composed its own local points cloud. A local points cloud consists of the selected neighboring points of certain computational point. For the accuracy and the efficiency of the computation, an appropriate strategy of selecting points among the neighboring points is necessary. In this study, space is split into 18 sections, then the closest point to interested point in each split space is selected for local point cloud. The splitting method is as follows.

Consider a cube which has the computational point $P(x_o, y_o, z_o)$ as a center, and has Cartesian unit vectors normal to the each face. Then the equation of a plane which contains a face of the cube is expressed as Eq. (3)

$$ax + by + cz + d = 0 \quad (3)$$

In Eq. (3) a , b , and c are the normal vector of a face of the cube, where $\langle a, b, c \rangle = \langle \pm 1, 0, 0 \rangle$, or $\langle 0, \pm 1, 0 \rangle$, or $\langle 0, 0, \pm 1 \rangle$, then d is given by

$$d = -(ax' + by' + cz') \quad (4)$$

Where x' , y' and z' are any point on the face. Basically, space is split into six by the faces of a cube. In order to divide space into eighteen, every faces of the cube are to be divided into five pieces. To divide the faces, let the coordinates of the center of one face be $Q \langle x_{fc}, y_{fc}, z_{fc} \rangle$, and the coordinates of one vertex of one face be $R \langle x_v, y_v, z_v \rangle$. Then let the point which internally divides line \overline{QR} into $a:b$ be $T \langle x_g, y_g, z_g \rangle$. The coordinates of T is given by Section formula for internal division. It is shown in Eq. (5)

$$\begin{aligned} x_g &= \frac{ax_v + bx_{fc}}{a + b} \\ y_g &= \frac{ay_v + by_{fc}}{a + b} \\ z_g &= \frac{az_v + bz_{fc}}{a + b} \end{aligned} \quad (5)$$

There are the four points of internal division for one face and four vertices which can be expressed as Eq. (5). Then, one square is formed by the points of internal divisions, and by connecting each vertex and the corresponding points of internal division, the four trapezoids are formed as illustrated in Fig. 3.

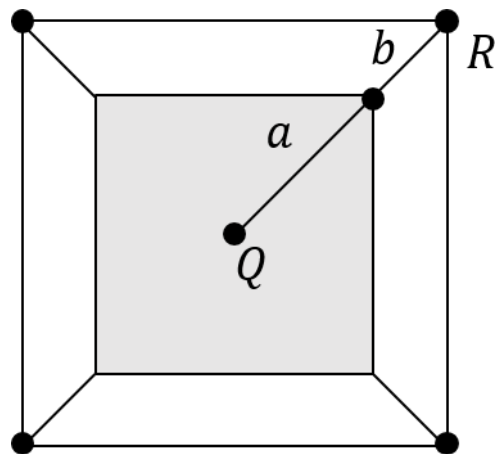


Fig. 3 The face divided into five pieces

Splitting every faces of the cube as previously described, the faces of the cube are divided into 30 zones. Consider two trapezoidal zones that sharing one side together as a one zone. Additionally, by letting $a:b = 1:(\sqrt{5} + 2)/2$, the cube are divided into 18 zones which have same area. It is shown in Fig. 4.

Consider a connecting line of the centroid point and a neighboring point that intersects the surface of the cube, an intersecting point can be matched to any of 18 divided surface. Then let the coordinates of the neighboring points be $S(x_n, y_n, z_n)$. Then the segment of line equation which connect the center and the neighboring point is written as Eq. (6).

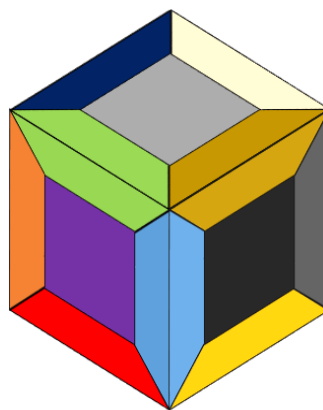


Fig. 4 The split zones

$$\frac{x - x_n}{x_n - x_o} = \frac{y - y_n}{y_n - y_o} = \frac{z - z_n}{z_n - z_o}, \text{ where } \begin{cases} \min(x_n, x_o) \leq x \leq \max(x_n, x_o) \\ \min(y_n, y_o) \leq y \leq \max(y_n, y_o) \\ \min(z_n, z_o) \leq z \leq \max(z_n, z_o) \end{cases} \quad (6)$$

By solving Eq. (3) and Eq. (6), the location of the intersecting point is determined. According to the position of the intersecting point, the zone where the neighboring point belongs is determined. In each divided zone, the closest neighboring

point is determined. Using these 18 points, the local points cloud of the center point is composed.

4. NUMERICAL METHOD

4.1 Least square method

In this study, least square method based on Taylor series expansion is used to get unknowns of partial derivative term represented on Eq. (7)

Ignoring high order terms, the Taylor expansion from the computational point $P(x_o, y_o, z_o)$ is denoted as

$$\varphi(x, y, z) = \varphi_0 + \Delta x \frac{\partial \varphi(x_o)}{\partial x} + \Delta y \frac{\partial \varphi(y_o)}{\partial y} + \Delta z \frac{\partial \varphi(z_o)}{\partial z} + O(\Delta^2) \quad (7)$$

The least square method with weighted function can be expressed as follows.

$$\min \sum_{j=1}^n \omega_{oj} \left[\Delta \varphi_{oj} - \Delta x_{oj} \frac{\partial \varphi(x_o)}{\partial x} - \Delta y_{oj} \frac{\partial \varphi(y_o)}{\partial y} - \Delta z_{oj} \frac{\partial \varphi(z_o)}{\partial z} \right]^2 \quad (8)$$

$$\frac{\partial \varphi}{\partial x} \approx \sum_j a_{oj} (\varphi_j - \varphi_o) \quad (9)$$

$$\frac{\partial \varphi}{\partial y} \approx \sum_j b_{oj} (\varphi_j - \varphi_o) \quad (10)$$

$$\frac{\partial \varphi}{\partial z} \approx \sum_j c_{oj} (\varphi_j - \varphi_o) \quad (11)$$

Where j is the index of the point in the cloud.

For a 3-D case, values of the coefficients are calculated as follows

$$AX = B \quad (12)$$

Where $X^T = [a_k \ b_k \ c_k]$, A and, B are denoted in Eq. (13)

$$A = \begin{bmatrix} \Sigma \omega \Delta x^2 & \Sigma \omega \Delta x \Delta y & \Sigma \omega \Delta x \Delta z \\ \Sigma \omega \Delta x \Delta y & \Sigma \omega \Delta y^2 & \Sigma \omega \Delta y \Delta z \\ \Sigma \omega \Delta x \Delta z & \Sigma \omega \Delta y \Delta z & \Sigma \omega \Delta z^2 \end{bmatrix}$$

$$B^T = [\Sigma \omega \Delta x \Delta \varphi, \Sigma \omega \Delta y \Delta \varphi, \Sigma \omega \Delta z \Delta \varphi] \quad (13)$$

Using inverse matrix of A , X can be derived.

For improving accuracy, a simple inverse distance weighting function is used. It

is represented on Eq. (14)

$$\omega_{0j} = \frac{1}{(\Delta x^2_{0j} + \Delta y^2_{0j} + \Delta z^2_{0j})^{1/2}} \quad (14)$$

4.2 Governing equation

Euler equations in strong conservation form are denoted in a Cartesian coordinate system for

$$\frac{\partial \omega}{\partial t} + \frac{\partial e}{\partial x} + \frac{\partial f}{\partial y} + \frac{\partial g}{\partial z} = 0 \quad (15)$$

$$\omega = \begin{bmatrix} \rho \\ \rho u \\ \rho v \\ \rho w \\ E \end{bmatrix}, \quad e = \begin{bmatrix} \rho u \\ \rho u^2 + P \\ \rho uv \\ \rho uw \\ \rho uE \end{bmatrix}, \quad f = \begin{bmatrix} \rho v \\ \rho uv \\ \rho v^2 + P \\ \rho vw \\ \rho vE \end{bmatrix}, \quad g = \begin{bmatrix} \rho w \\ \rho uw \\ \rho vw \\ \rho w^2 + P \\ \rho wE \end{bmatrix} \quad (16)$$

In Eq. (16), E represents a total energy as follows

$$E = \frac{P}{(\gamma - 1)\rho} + \frac{1}{2}(u^2 + v^2 + w^2) \quad (17)$$

5. NUMERICAL RESULT

5.1 flow around NASA X TM 2059 without a nozzle

In order to conduct a validation of the meshless point generation method, numerical results on the supersonic flow around a missile body obtained using meshless method and finite volume method with unstructured grid were compared. The numerical schemes and the flow conditions are described in Table 1.

Table 1 Numerical schemes and the flow conditions

| Method | Meshless | Unstructured |
|----------------------------|----------------|--------------|
| Spatial discretization | AUSMPW+ | AUSM |
| Time integration | LU-SGS | Explicit |
| Number of points | 3,040,247 | - |
| Number of cells | - | 2,288,459 |
| model | NASA X TM 2059 | |
| Freestream Mach number | 2.5 | |
| Freestream pressure (Pa) | 100,000 | |
| Freestream temperature (K) | 300 | |
| Angle of attack (degree) | 0 | |

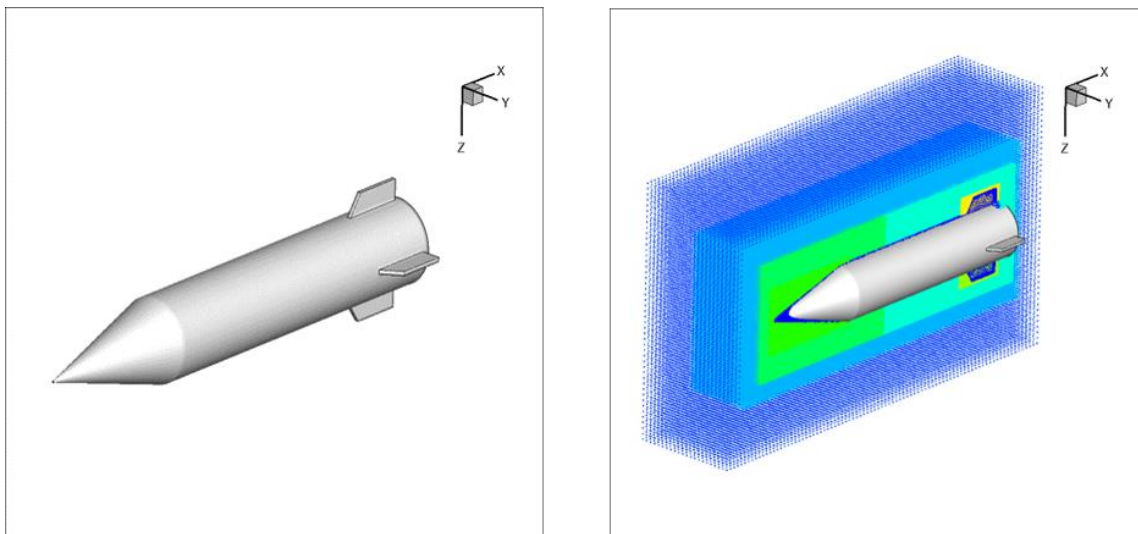


Fig. 5 The figuration of NASA X TM 2059 (left) and the computational domain of NASA X TM 2059 (right)

As a missile body, NASA X TM 2059 model was selected. Additionally the four tail fins are attached to this body. The figuration of missile body and the generated meshless point system is shown in Fig. 5. The meshless method used AUSMPW+, and FVM used AUSM. Fig. 6 shows the pressure contour at $z=0$ computed by using the meshless method and FVM. Fig. 7 shows pressure distribution along the line $y=0.15$ at $z=0$ respectively. Lastly Fig. 8 shows the convergence history of two methods. As it is shown in Fig.6 ~7, it has been observed that the results of the meshless method is similar those of FVM.

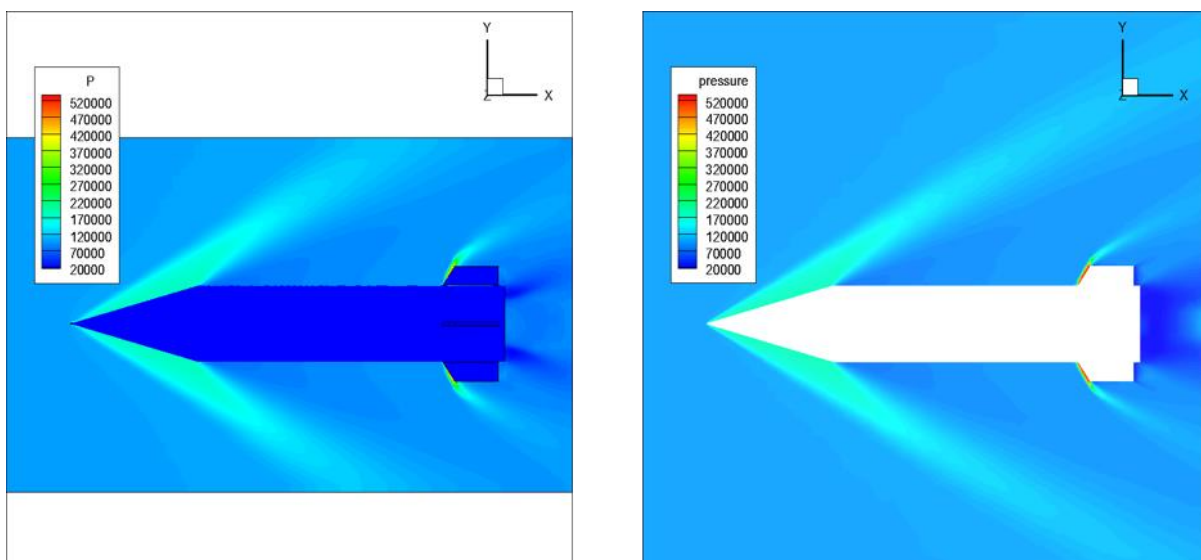


Fig. 6 The pressure contour of each method (left: meshless, right: FVM)

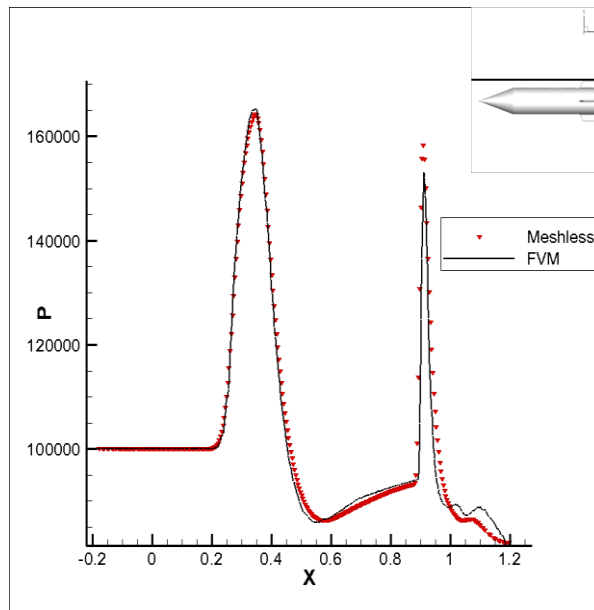


Fig. 7 The comparison of the pressure distribution along $y=0.15$ at $z=0$

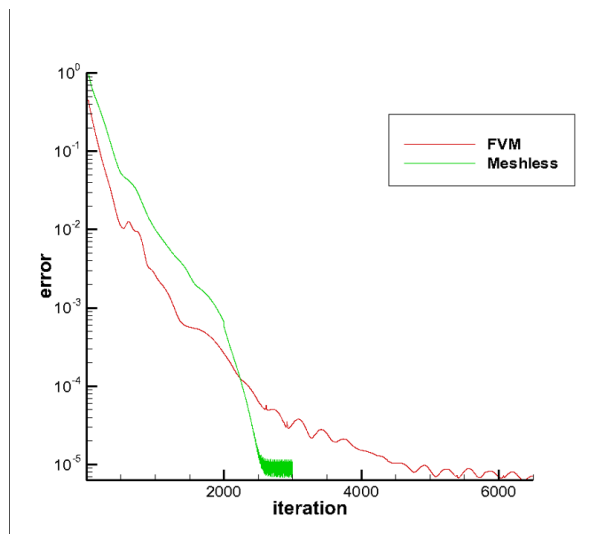


Fig. 8 The comparison of the convergence history

5.2 flow around NASA X TM 2059 with nozzle and vane

One of the validation cases, the reformed NASA X TM 2059 model is considered. In order to integrate the external flow and the internal flow, Twenty-degree conical nozzle (Burt 1971) and vanes are added to the previous model. Fig. 9 illustrated the figuration of the reformed model and the computational domain. At the condition altitude 10km, the computation was conducted. The numerical schemes and the flow conditions are described in table 2.

Table 2 Numerical schemes and the flow conditions

| | | |
|--------------------------|--|--------------------|
| Method | Meshless | |
| Spatial discretization | AUSMPW+ | |
| Time integration | LU-SGS | |
| Number of points | 3,303,803 | |
| model | NASA X TM 2059 with a nozzle and vanes | |
| Freestream Mach number | 5 | |
| | Free stream | Combustion chamber |
| pressure (Pa) | 26,500 | 700,000 |
| temperature | 223 | 3,000 |
| species | air, plume | |
| Angle of attack (degree) | 0 | |

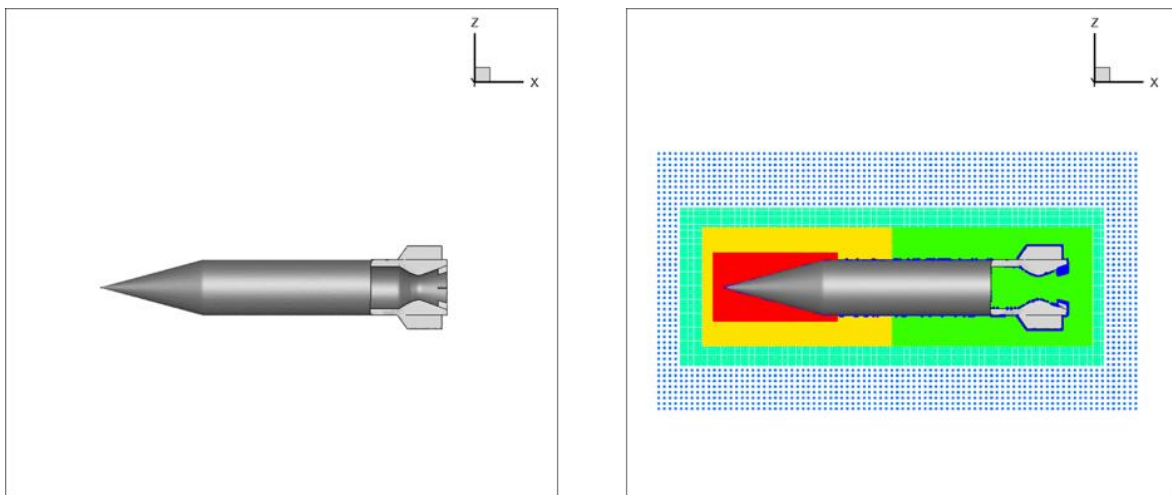


Fig. 9 The figuration of reformed model (left) and the computational domain (right)

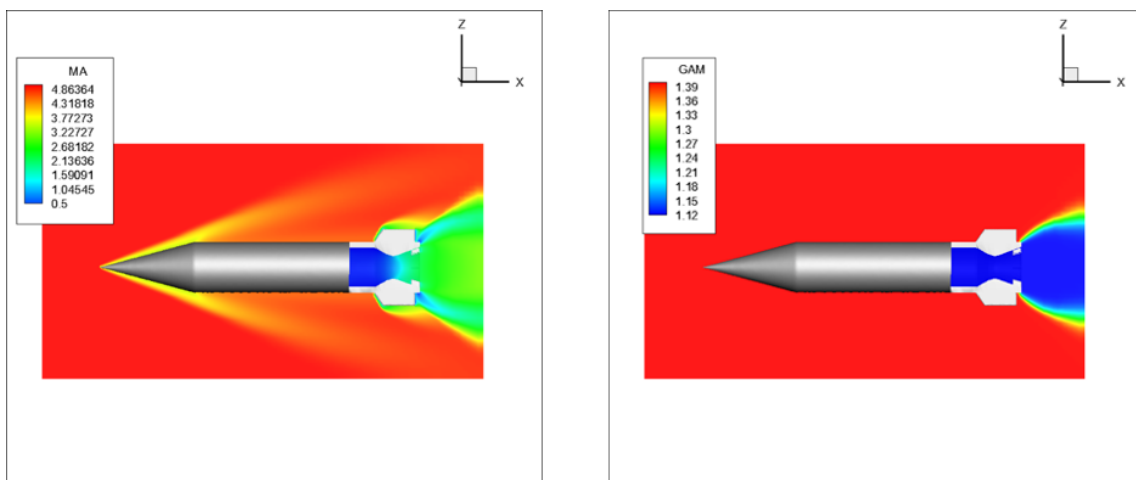


Fig. 10 Mach number contour (left) and heat of ratio contour (right)

Fig. 10 illustrates results of computations. The right contour denotes the Mach number contour and the left result denotes the heat of ratio contour. From the Mach number contour, Mach number varies along the nozzle area. And the heat of ratio contour shows that the plume flows out from the nozzle. Lastly, Fig. 11 denotes the convergence history. These results show that even if a figuration is complicated, the developed technique is still available.

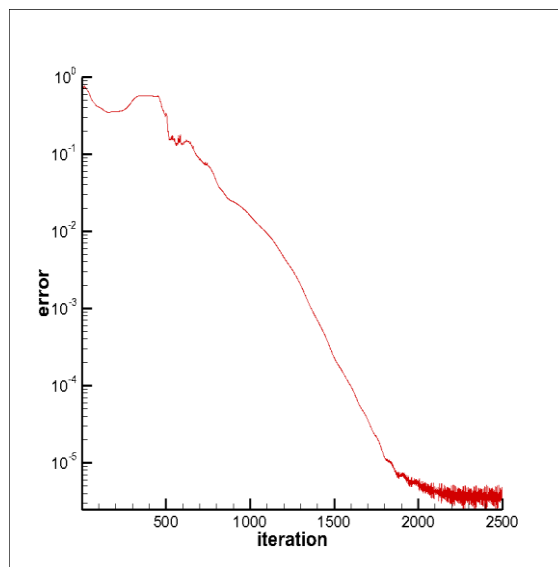


Fig. 11 The convergence history

3. CONCLUSIONS

In this study, the meshless point generation technique which generates computational domain and the local points cloud is developed. The numerical results of comparison with FVM indicate the meshless point generation technique and the meshless method have similar robustness, accuracy to those of unstructured finite volume method. Additionally, by analyzing the flow field around NASA TM X 2059 which has a nozzle and vanes using meshless point generation technique, the robustness of this technique is confirmed.

REFERENCES

- Burt Jr, J. R. (1971). An Investigation of the Effectiveness of Several Devices in Simulating a Rocket Plume at Free Stream Mach Numbers 0.9 to 1.2 (No. RD-TR-71-22). ARMY MISSILE COMMAND REDSTONE ARSENAL ALA AEROBALLISTICS DIRECTORATE.
- Huh, J., Kim, K., & Jung, S. (2013). Meshless Method for Simulation of 2-D Compressible Flow. In The 2013 Asia-Pacific International Symposium on Aerospace Technology.

- Katz, A., & Jameson, A. (2009). A comparison of various meshless schemes within a unified algorithm. AIAA paper, 594.
- Kim, K. H., Kim, C., & Rho, O. H. (2001). Methods for the accurate computations of hypersonic flows: I. AUSMPW+ scheme. *Journal of Computational Physics*, 174(1), 38-80.